Model of Crystallization in a Confined Space Applied to Iron Uptake and Release by Ferritin

Anne Courteix
IUT Département de Chimie, Université Paul Sabatier, 81100 Castres, France

Alain Bergel
Laboratoire de Génie Chimique, Université Paul Sabatier, 31062 Toulouse, France

Many living organisms store iron in solid form, Fe(III), as a crystal in the inner cavity of the ferritin molecule. When iron is needed for biosynthesis, a reducing agent reduces Fe(III) into the soluble form Fe^{2+} released by ferritin. Crystallization and release processes are reversible, and their rates evolve in an identical way as a function of the number n of iron atoms in the molecule. The rate increases with n, showing a maximum value when n is approximately 1,300, and then stabilizes for the highest values of n, which can reach 4,500. On the other hand, plotting the amount of released iron as a function of time gives curves with a sigmoid shape. The proposed model was based on the theoretical description of different steps involved in crystal growth inside the protein shell: several independent crystals grow freely at the inner protein wall, and then a distribution function takes into account possible overlapping of different crystallite clusters, whose further growth is limited by diminution of the available space inside the cavity. The kinetics derived was then used to calculate the release curve as a function of time. Solving the system of differential mass-balance equations was simplified by describing the ferritin population as a large discrete distribution of species. The model fully fitted and explained the variation in the crystallization rate with n, and the sigmoid shape of the release curve as a function of time obtained experimentally in a thin-layer electrochemical cell.

Introduction

Chemical engineering methods have brought substantial contributions to biomedical engineering or to fundamental research in the life sciences. Numerous significant examples highlight the variety of fundamental topics investigated: general aspects of momentum and mass transport (Lightfood, 1974); water flow across alveolar epithelium (Kim and Crandall, 1983); pulmonary blood flow (Saidel and Burma, 1983); physicochemical properties of human tissue cells (DiMilla et al., 1992); or of human skin (Steven et al., 1993). The purpose of this work is to elaborate a model of crystallization inside a confined space to be applied to the kinetics of iron storage and release in living organisms.

In most living organisms iron is stored in solid form as Fe(III), which is barely soluble (solubility constant 10^{-37}). Thus, these organisms have sequestering molecules, ferritins, that maintain the iron in a stable form where it is available for transport or haem synthesis. Ferritin is found especially in the liver, spleen, and bone marrow of mammals (Macara et al., 1972). It is, however, widely distributed in vertebrates, invertebrates, bacteria (Chasteen and Theil, 1982) or in the vegetable kingdom (phyto- or mycoferritin) (Hoffmann and Harrison, 1963). Ferritin molecules are made up of a protein shell, called apoferritin, and a microcrystallite core, or micelle, situated within the hollow shell and containing up to about 4,500 iron atoms (Harrison et al., 1967). The whole molecule approximates a rhombic dodecahedron yielding an inner spherical iron-storage cavity of about 70 to 80 Å in diameter. The shell, with an approximate molecular weight of 480,000, consists of 24 subunits designated *H* (for heavy, with molecular weights about 21,000) and *L* (for light, with molecular weights about 19,000) (Adelmann et al., 1975; Arosio et al., 1978; Ford et al., 1984). The proportion of the two subunits differs depending on the tissue source of the protein.

The general iron uptake and release mechanism is now well

established. Fe^{2+} ions enter the protein shell through channels and are oxidized into Fe(III), which form a polynuclear ferric oxyhydroxide core associated with some phosphate (Harrison et al., 1967). The threefold and fourfold symmetry axes of the molecule are pierced by channels that allow Fe^{2+} and perhaps some other small molecules to move toward the central cavity. It seems that the threefold channels are preferentially used as passageway by iron, although they may not be the only route (Treffy et al., 1993). The protein shell plays an integral part in iron core formation. Fe^{2+} complexation by the protein is followed by oxidation to Fe(III) at protein ferroxidase sites (Lawson et al., 1989). Examination of the three-dimensional structure of human ferritin has showed a pathway lined with hydrophilic residues between the threefold channels and the ferroxidase centers (Treffy et al., 1993). The ferroxidase activity is associated with *H*-subunits, while the *L*-subunits, devoid of ferroxidase sites, better fulfill a long-term storage function (Lawson et al., 1991). Phosphate is involved in the core structure in very different proportions depending on the origin of the ferritin (Watt et al., 1986; Harris et al., 1994). For instance, ratios of iron uptake with respect to inorganic phosphate as different as 1.71 for bacterial ferritin and 21.0 for human ferritin have been determined (Mann et al., 1986).

Iron release occurs through the action of a reducing agent that transforms the Fe(III) core into soluble Fe^{2+} ions. Iron release has been the focus of numerous studies that used either a strong reducing agent, such as dithionite, or other reducers, such as superoxide anions $O_2^{\cdot-}$ (Monteiro et al., 1989), reduced flavins (Sirivech et al., 1974; Imai et al., 1980), or viologens (Jacobs et al., 1989). It is not clear whether the reducing molecule penetrates the protein shell by some of the channels or if a long-range electronic transfer occurs through the shell (Kadir et al., 1991; Kadir et al., 1992).

The processes of iron uptake or release are reversible. Their rates vary in the same way as a function of the number *n* of iron atoms contained in the molecule. Plotting this rate as a function of *n* always gives the same curve shape, no matter what the experimental conditions are. The rate increases, reaches a maximum for a number of atoms of the order of 1,300, decreases, then stabilizes (Figure 1). Plotting

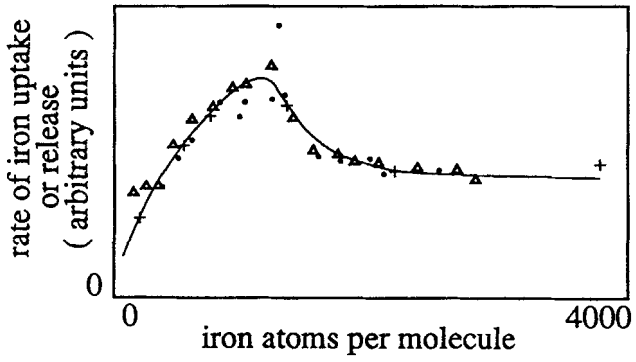

Figure 1. Uptake and release rates as a function of iron content, experimental results.

Experimental results from Harrison et al. (1974). • Uptake of iron added as $(NH_4)_2Fe(SO_4)_2$ with an excess of KIO_3-$Na_2S_2O_3$; △ uptake of iron added as $(NH_4)_2Fe(SO_4)_2$ with an excess of molecular O_2; + iron release with 1,10-phenanthroline.

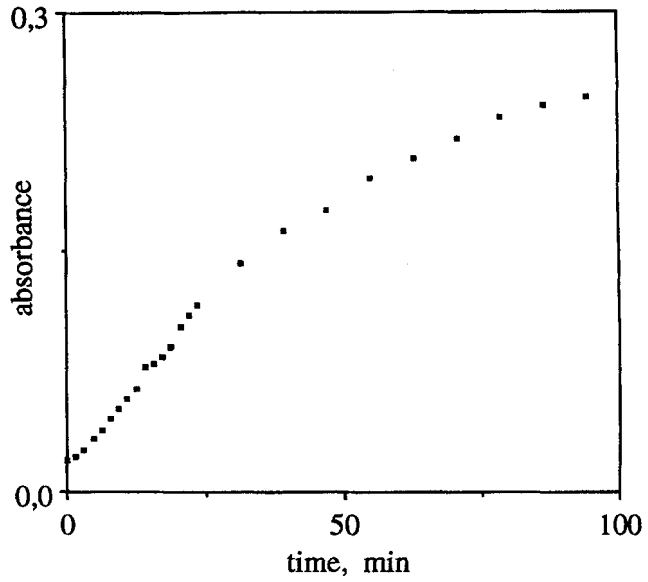

Figure 2. Iron release as a function of time, experimental results.

Experiment was carried out in a thin-layer electrochemical cell in tris-HCl 25 mM, pH 7.4 buffer, with 1 g/L ferritin, 0.2 mM FMN, and an excess of 2,2′-bipyridine.

the amount of released iron vs. time usually gave a sigmoid shape curve (Figure 2).

In order to explain these kinetics, two different types of investigative approach have been proposed. On the one hand, the most numerous works have been of a purely biochemical nature. They have given a wealth of information concerning the structure, mechanism, and influence of some parameters such as the phosphate ratio or the ferritin source. On the other hand, physical studies assumed that kinetics are essentially controlled by variation of the accessible area during crystal growth or solubilization (Macara et al., 1972; Harrison et al., 1974). The current trend seems to accept that one or the other explanation predominates, depending on the experimental conditions (Ford et al., 1984; Levi et al., 1988). Sun and Chasteen (1992) suggested a different stoichiometry according to the uptake being performed with small or great iron increments. With iron increments not exceeding 50 atoms per protein molecule, oxidation essentially occurred via the ferroxidase sites. On the contrary, with increments of about 240 to 960 atoms per protein molecule iron is initially oxidized on the protein but once sufficient core has developed, iron oxidation and deposition occurs directly on the core surface.

Nevertheless, compared to the numerous biochemical studies, kinetic physical investigations remain very poor. The old and simple crystal growth model based on a single spheric crystal is still used, although it does not fit the experimental data.

The aim of this article is to improve the physical model of iron crystallization or release by adapting some well-known concepts of chemical engineering to the particular case of crystallization in a confined space. The changes in the rate of iron release vs. the amount *n* of iron contained in the protein could thus be totally and quantitatively explained by the constraint imposed by the protein shell on core formation. Since

ferritin molecules react with different rates depending on the number of iron atoms they contain, it is necessary to consider them as a discrete population in the balance equations, as would be the case for classic crystal at different stages of crystallization. Coupling crystallization kinetics with mass transfer then makes it possible to fully explain the sigmoid shape of iron release curves as a function of time. Some experimental results obtained by electrochemical reduction of ferritin can thus be explained without recourse to any other hypothesis.

Experiment

Experimental data concerning the variations in uptake and release rates as a function of the number n of iron atoms contained in the ferritin molecule were taken from Harrison et al. (1974).

The iron release curves as a function of time were obtained in the laboratory and have already been published (Durliat et al., 1993). Experiments were carried out in a thin-layer electrochemical cell with flavin mononucleotide (FMN) as reducing agent. The reduced form of flavin was continuously regenerated by a very fast reaction at the platinum cathode maintained at the potential -0.45 V with respect to a saturated calomel reference electrode (SCE). By using a thin-layer cell it was possible to monitor absorbance of the solution continuously. A detailed description of the experimental setup has already been published elsewhere (Durliat and Comtat, 1982). Experiments were performed in tris-HCl 25 mM, pH 7.4 buffer containing 1-g/L horse spleen ferritin, 0.20-mM FMN, and an excess of 2,2′-bipyridine. 2,2′-Bipyridine was used to form a complex with released Fe^{2+} whose absorbance can be easily monitored at 520 nm ($\epsilon = 8{,}430\ M^{-1}\cdot cm^{-1}$).

Horse spleen ferritin and FMN were purchased from Sigma. A Princeton Applied Research EGG 362 potentiostat and a Hewlett-Packard 8451 diode array spectrophotometer were used. The numerical program was written in Fortran and fed to a Hewlett-Packard 9000 workstation.

Theory

Crystallization rate as a function of iron content n

The processes of iron storage and release by ferritin are reversible. The rate of iron crystallization or release varies in the same way as a function of the number n of iron atoms contained in the protein. Whatever the experimental conditions, the curve showing rate as a function of n always exhibits the shape plotted in Figure 1. The fundamental assumption of all physical interpretations is that rate variation is due to the variation of the accessible core surface. Despite many improvements the first models based on crystallization of a single spherical or hemi-spherical crystal did not satisfactorily fit the experimental data (Hoy et al., 1974; Jones et al., 1978).

Based on the bibliographic analysis, hypotheses were retained that described the crystallization process as it would occur, for instance, in the interior of a geode in mineralogy:

- A polynuclear core is formed by crystallization at different sites on the inner surface of the protein.
- Each crystal grows toward the center, at first freely, then impeded by the bordering crystals. The part of the crystal surface that is turned toward the protein wall becomes inaccessible.
- The growth stops when the access channels are blocked by the crystal.

The crystals grow individually from the protein wall toward its center. When they collide their lateral growth is blocked but they continue to grow with a deformed surface. The decrease in the accessible surface is calculated in proportion to the available surface in the sphere. An equivalent radius r_e is defined as the internal radius that would be attained if all the iron atoms uniformly covered the protein wall. The accessible surface of the laterally blocked crystals decreases proportionally to r_e^2. Once a crystal is laterally blocked by the bordering crystals, the sides that face the protein wall can no longer be reached by new iron atoms. Half of its surface therefore becomes inaccessible for further growth. The total accessible surface S thus equals the sum of the areas of the independent crystals and half of the deformed areas of the laterally blocked crystals:

$$S = N_c(1-\psi)A + 0.5\, N_c \psi A \frac{r_e^2}{R^2}, \tag{1}$$

where N_c is the number of crystals, ψ the proportion of blocked crystals, A the area of one crystal, r_e the equivalent radius, and R the radius of the inner cavity of the protein.

Let us define h as the characteristic size of the crystal, the shape of a crystal or a cluster is correlated to h by three shape factors u, v, w:

- Crystal volume $= uh^3$ (2)
- Accessible crystal area: $A = vh^2$ (3)
- Projected area of one crystal onto the shell wall $= wh^2$ (4)

Using the average atomic volume of one crystal V to express the total volume occupied by the crystals:

$$nV = N_c u h^3 \tag{5}$$

allowed h to be calculated as a function of iron content n:

$$h = \left(\frac{nV}{uN_c}\right)^{1/3}. \tag{6}$$

Similarly, the equivalent radius r_e is derived from the expression of the total volume occupied by the crystals:

$$nV = \frac{4}{3}\pi(R^3 - r_e^3) \tag{7}$$

$$\frac{r_e}{R} = \left(1 - \frac{3nV}{4\pi R^3}\right)^{1/3}. \tag{8}$$

In all the equations, the average atomic volume V is calculated by using the volumic filling ratio F, defined as the pro-

portion of the protein occupied when crystallization is completed:

$$V = \frac{4\pi R^3}{3 \cdot 4{,}500} F. \tag{9}$$

Blocking of the channels before the protein cavity was totally filled induced F values less than 1.

Let us define h^* as the maximum value beyond which all the crystals would be contiguous:

$$4\pi R^2 = N_c w h^{*2}. \tag{10}$$

If the crystallization sites were uniformly distributed along the protein surface, ψ would be equal to zero so long as h remained less than h^*, because all the crystals grew independently, while ψ would equal one when h reached h^*. Because of a random distribution of the crystallization sites, ψ was assumed to be the normal distribution associated with a Gaussian function centered on h^* and with a standard deviation σ:

$$\psi(h) = \frac{1}{2} \int_{-\infty}^{(h-h^*)/\sigma} \exp\left(\frac{-x^2}{2}\right) dx. \tag{11}$$

Finally, the parameters of the model were

- F the volumic filling ratio of the protein when it contains 4,500 iron atoms
- N_c the number of crystallization sites
- σ the standard deviation of the distribution of crystallization sites
- u, v, w the crystal shape factors, which were directly calculated on the basis of the chosen crystal geometry

Iron release as a function of time

Because of the variation in the Fe^{2+} release rate with respect to the iron content n, it was necessary to consider ferritin as a population composed of $N+1$ distinct species (noted Iron_n), N being the maximum number of iron atoms contained in the ferritin cavity. Each ferritin species Iron_n underwent a reaction with reduced flavin (reduction agent noted Red) yielding free Fe^{2+}, the ferritin species Iron_{n-1} and oxidized flavin (Ox). In the thin-layer electrochemical cell the reduced form of flavin was continuously regenerated by oxidation of Ox at the electrode surface.

It is generally accepted that diffusion phenomena are negligible in a thin-layer electrochemical cell, since the thickness of the cell is of the same magnitude as that of a diffusion layer. Nevertheless, this hypothesis is not used here because it is not valid when the rate of the homogeneous reactions is too high (Devaux et al., 1995). The theoretical description of the cell is classic (Hubbard and Anson, 1970): the electrode is a plane surface that defines one side of the cell ($x = 0$), with the other side being determined by an inert surface ($x = \delta$).

The differential mass balance relative to each ferritin species reacting with the reduction agent (Red) gives:

$$\frac{\partial[\text{Iron}_n]}{\partial t} = D_{\text{Iron}} \frac{\partial^2[\text{Iron}_n]}{\partial x^2} - k_n[\text{Red}][\text{Iron}_n] + k_{n+1}[\text{Red}][\text{Iron}_{n+1}] \tag{12}$$

for $0 \le n < N$ and with $k_0 = 0$.

The kinetic term is the difference between the rate at which the ferritin species Iron_n disappears and the rate at which it appears through transformation of the species Iron_{n+1}. For $n = N$ the equation becomes

$$\frac{\partial[\text{Iron}_N]}{\partial t} = D_{\text{Iron}} \frac{\partial^2[\text{Iron}_N]}{\partial x^2} - k_N[\text{Red}][\text{Iron}_N], \tag{13}$$

since there is no creation of the species Iron_N. The diffusion coefficients are assumed to be equal for all the ferritin species. The rate of consumption through chemical reaction of the reduction agent (reduced flavin) is the sum of all the reactive terms of iron release:

$$\frac{\partial[\text{Red}]}{\partial t} = D_{\text{Red}} \frac{\partial^2[\text{Red}]}{\partial x^2} - \left(\sum_{n=1}^{N} k_n[\text{Red}][\text{Iron}_n] \right). \tag{14}$$

Boundary conditions are imposed by the electrochemical reactions at the electrode surface ($x = 0$). Mass fluxes of ferritin species are nil, since they are not electroactive:

$$\frac{\partial[\text{Iron}_n]}{\partial x} = 0 \qquad 0 \le n \le N. \tag{15}$$

The reduction rate of flavin is assumed to be very high compared with diffusion rates, and the diffusion coefficients of the oxidized and reduced forms of flavin are assumed to be equal. Consequently, the boundary condition at the electrode surface is

$$[\text{Red}] = [\text{FMN}]^0, \tag{16}$$

where $[\text{FMN}]^0$ is the initial flavin concentration.

At the cell wall ($x = \delta$) all the mass fluxes are nil:

$$\frac{\partial[\text{Iron}_n]}{\partial x} = 0 \qquad \frac{\partial[\text{Red}]}{\partial x} = 0. \tag{17-18}$$

Using dimensionless variables, the system to be solved becomes

$$\frac{\partial C_n}{\partial T} = Di \frac{\partial^2 C_n}{\partial X^2} - K_n C_{\text{Red}} C_n + K_{n+1} C_{\text{Red}} C_{n+1} \qquad 0 \le n < N \tag{19}$$

$$\frac{\partial C_N}{\partial T} = Di \frac{\partial^2 C_N}{\partial X^2} - K_N C_{\text{Red}} C_N \tag{20}$$

$$\frac{\partial C_{\text{Red}}}{\partial T} = \frac{\partial^2 C_{\text{Red}}}{\partial X^2} - C_{\text{Red}} \left(\sum_{n=1}^{N} K_n C_n \right). \tag{21}$$

At $X=1$:

$$\frac{\partial C_n}{\partial X}=0 \qquad 0\le n\le N. \tag{22}$$

$$C_{\text{Red}}=1. \tag{23}$$

At $X=1$:

$$\frac{\partial C_n}{\partial X}=0 \qquad 0\le n\le N \tag{24}$$

$$\frac{\partial C_{\text{Red}}}{\partial X}=0. \tag{25}$$

Initial conditions:

$$C_n=0 \qquad 0\le n< N \tag{26}$$

$$C_N=C^0 \tag{27}$$

$$C_{\text{Red}}=0, \tag{28}$$

which implies integration of $N+2$ equations.

The system can be significantly simplified by grouping the ferritin species by bands of width Δn, within which the concentration is assumed to be constant and equal to that of the center of the band. Letting Γ_i be the sum of the concentrations of species containing from $(i-1)\Delta n+1$ to $i\Delta n$ iron atoms, Γ_i is expressed

$$\Gamma_i=\Delta n\, C_{n(i)}, \tag{29}$$

where

$$n(i)=i\Delta n-\frac{\Delta n}{2}+0.5. \tag{30}$$

Summation of the Δn equations composing a band yields

$$\frac{\partial \Gamma_i}{\partial T}=Di\frac{\partial^2\Gamma_i}{\partial X^2}-\frac{K_{n(i)}}{\Delta n}C_{\text{Red}}\Gamma_i+\frac{K_{n(i+1)}}{\Delta n}C_{\text{Red}}\Gamma_{i+1}. \tag{31}$$

For the singular values $n=0$ and $n=N$, let

$$\Gamma_0=C_0 \qquad \text{and} \qquad \Gamma_i=C_N, \tag{32}$$

with

$$I=\frac{N-1}{\Delta n}+1. \tag{33}$$

It should be noted that this calculation assumes that $(N-1)$ is divisible by Δn. If this is not the case, a larger number of singular values must be used in order for I to remain an integer. The system thus consists of $[(N-1)/\Delta n]+4$ equations:

$$\frac{\partial \Gamma_i}{\partial T}=Di\frac{\partial^2\Gamma_i}{\partial X^2}-\frac{K_{n(i)}}{\Delta n}C_{\text{Red}}\Gamma_i+\frac{K_{n(i+1)}}{\Delta n}C_{\text{Red}}\Gamma_{i+1} \qquad 0\le i<I \tag{34}$$

$$\frac{\partial \Gamma_I}{\partial T}=Di\frac{\partial^2\Gamma_I}{\partial X^2}-k_N C_{\text{Red}}\Gamma_I \tag{35}$$

$$\frac{\partial C_{\text{Red}}}{\partial T}=\frac{\partial^2 C_{\text{Red}}}{\partial X^2}-C_{\text{Red}}\left(\sum_{i=1}^{I}K_{n(i)}\Gamma_i\right). \tag{36}$$

The boundary and initial conditions remain the same.

The system was solved numerically by an implicit Crank and Nicholson finite difference method. The nonlinear kinetic term was evaluated by the sum

$$\frac{K_{n(i)}\Gamma(T)C_{\text{Red}}(T)}{2\Delta n}+\frac{K_{n(i)}\Gamma(T+\Delta T)C_{\text{Red}}(T+\Delta T)}{2\Delta n}.$$

Occurrence of a nonlinear term expressed at time $T+\Delta T$ implies iterations for every time step. The use of an underrelaxation method to correct the value calculated at $T+\Delta T$:

$$\Gamma(T+\Delta T)^{\text{new}}=\Gamma(T)+0.5[\Gamma(T+\Delta T)-\Gamma(T)] \tag{37}$$

improved the convergence of these iterations. The sum of the absolute values of all the concentration differences between two consecutive iterations was chosen as the stop criterion. When its value became less than 10^{-5}, calculation went to the next time step.

The concentration profiles obtained were integrated from $X=0$ to $X=1$ to have the average concentration of each species within the cell. The sum of these concentrations for all the ferritin species should remain equal to the initial concentration C^0_{Iron}. Conservation of the total ferritin amount was thus verified for each time step. The only values that are experimentally accessible are flavin and Fe^{2+} concentrations in solution. The latter, denoted $C_{\text{Fe(II)}}$, was calculated as the difference between the total iron concentration and the concentration of iron contained in all the ferritin species:

$$C_{\text{Fe(II)}}=NC^0_{\text{Iron}}-\left[\sum_{i=1}^{I}n(i)\Gamma_i\right]. \tag{38}$$

Results

Crystallization rate as a function of iron content n

Three forms of crystal or cluster were considered: spheric, cubic, and octahedral; the corresponding shape factors u, v, and w are reported in Table 1. In the two latter cases, w was calculated by assuming that the crystal was in contact with the protein wall by one of the edges of the cube or one of the peaks of the octahedre. The successive determination of V, h, r_e, and ψ as a function of n, using Eqs. 5 through 11 led to the accessible surface expressed by Eq. 1 as a function n.

For each crystal shape a group of parameters (N_c, F, σ) was found by a trial-and-error method that correctly fitted the experimental data (Figure 3). Each parameter exerted a preponderant influence on a specific part of the release curve. The number of crystallization sites N_c largely determined the position of the maximum in the curve. It varied from $n=1{,}340$ to $n=920$ when N_c increased from 10 to 20. The standard deviation σ essentially allowed the decreasing part to be ad-

Table 1. Shape Factors of the Crystals or Clusters

Shape	Size h	u Vol.	v Area	w Proj. Area
Cubic	Side	1	6	$\sqrt{2}$*
Octahedral	Half-height	4/3	$4\sqrt{3}$	2†
Spheric	Radius	$4\pi/3$	4π	4π

*Contact by one of the cube edges.
†Contact by one of the peaks.

justed. The last part of the curve was a function of the filling ratio F. The accessible surface, and consequently the uptake or release rates, tended toward zero for the high values of n as F approaches 1. A good fitting of the experimental data was obtained for similar values of σ and F for the three types of crystals. Only N_c should vary and be adjusted over a wide range of values. The values of 350 and 500 found for the cubic and octahedral crystals, respectively, appeared to be far too high. The value of 15 found for the spheric cluster seems more realistic. The crystalline cluster should consequently have a rather compact form close to the spheric form. It has also to be noted that the value of 15 is of the same order of magnitude as the number of L-subunits that fulfill the iron storage function.

It is worth noting that the model allowed fitting of the whole release curve, and that it correlated each part of the curve with a specific step of the crystallization process:

- Individual growth of the clusters leads to a fast increase of the accessible surface.
- Progressive aggregation of the clusters induces masking of a part of the surface, resulting in rate decaying.
- During growth as a whole of all the blocked clusters toward the center of the cavity the increase in surface prompted by the growth of each cluster is counterbalanced by the decrease of available surface. These two antagonist phenomena resulted in stabilization of the accessible crystal area.

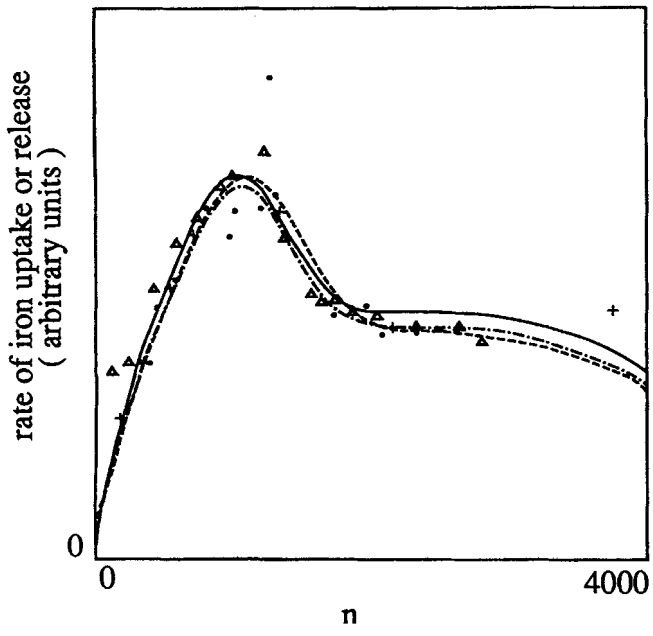

Figure 3. Theoretical effect of iron content on uptake and release rates.

------ cubic crystal, $N_c = 350$, $\sigma = 0.01$, $F = 0.9$; -·-·-· octahedral crystal, $N_c = 500$, $\sigma = 0.01$, $F = 0.9$; —— spheric cluster, $N_c = 15$, $\sigma = 0.02$, $F = 0.9$.

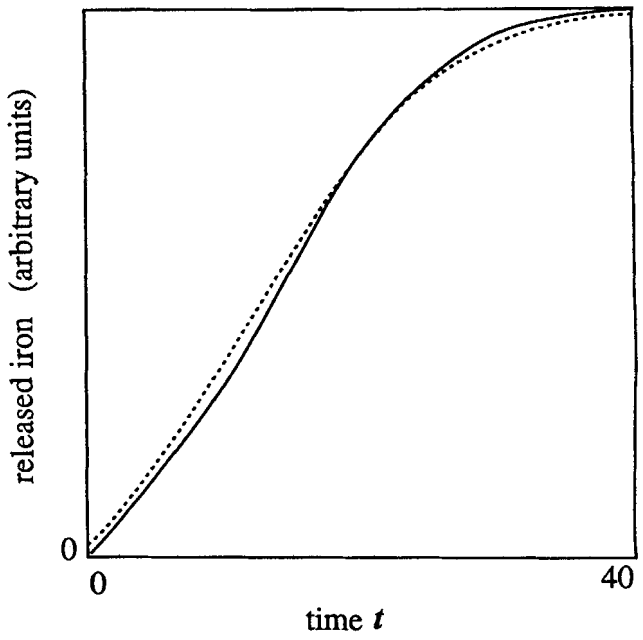

Figure 4. Iron release as a function of a time, effect of Δn.

$[\text{Iron}]^0 = 2.5\ 10^{-3}$; $N = 2{,}071$; ——, $\Delta n = 5$ and $\Delta n = 30$; ------, $\Delta n = 90$.

Iron release as a function of time

Stability of the algorithm was first verified by variation of the space and time steps and of the discretization steps of the ferritin population Δn. Values of 0.1 and 0.05 for ΔX and ΔT, respectively, assured a good convergence and allowed the conservation of the total ferritin amount to within 2%. The curve $C_{\text{Fe(II)}}$ as a function of time of Figure 4 was plotted with the experimental data: initial ferritin concentration $C^0_{\text{Iron}} = [\text{Ferritin}]^0/[\text{FMN}]^0 = 2.5\ 10^{-3}$, number of iron atoms initially contained in the ferritin molecules $N = 2{,}071$, and the set of k_n values derived from the experimental points of Figure 3. The curves plotted for $\Delta n = 5$ and $\Delta n = 30$ (solid line), that is, with 417 and 72 equations, respectively, are practically indistinguishable. The gain in calculation time was approximately proportional to the value of Δn compared to the program that solved all the 2,073 equations. The curve plotted for $\Delta n = 90$ (dashed line) is slightly removed from the preceding curves. It was thus chosen to use $\Delta n = 30$ for further calculations.

The evolution of the distribution of the iron content in the ferritin molecules is plotted for times $T = 6$, 12, 18, 24, and 30 in Figure 5. All the initial ferritin molecules were assumed to contain the same number of iron atoms ($N = 2{,}071$). During iron release, the distribution progressively widened. In contrast to the kinetic curves giving $C_{\text{Fe(II)}}$ as a function of time, Δn had a significant influence. Variation of Δn from 5 (dashed line) to 30 (solid line) logically provoked widening of the distribution curves. However, the curves remained centered around almost the same values, and the deformation was symmetric. This certainly explained invariance of the iron release curves plotted in Figure 4.

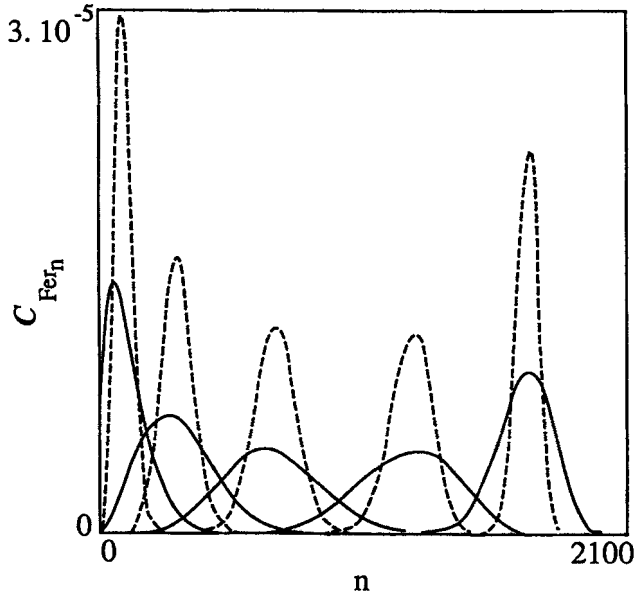

Figure 5. Effect of Δn on ferritin distribution.

[Iron]^0 = 2.5 10^{-3}; N = 2,071; -----, Δn = 5; ——, Δn = 30.

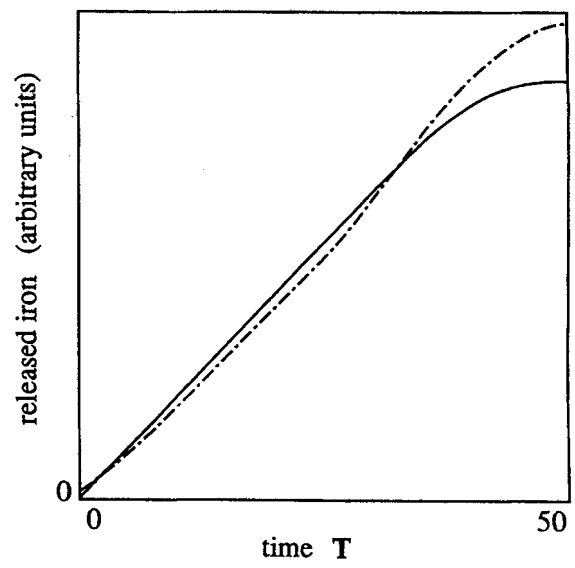

Figure 6. Iron release as a function of time, effect of the number of crystallization sites, and the variation of the rate constant with respect to n.

——, Similar to Figure 4 with all the K_n equal; -·-·-·, similar to Figure 4 with N = 4,500.

Figure 6 shows that with the same experimental conditions, but with ferritin initially completely filled (N = 4,500, dashed line), the sigmoid shape of the release curve is less apparent than in Figure 4 (N = 2,071). This approaches the results obtained by Funk et al. (1985), which have not observed the sigmoid form in experiments performed with completely filled ferritins. However, this analogy should be suggested with caution, because the experiments of Funk et al. were performed in a continuously stirred reactor, which is quite far from the conditions of the thin-layer cell used here. The curve obtained with all the K_n values taken equal is also plotted in Figure 6 (solid line). The sigmoid form totally disappeared, which proves that it is induced by the special variation of K_n as a function of n. The model is thus fully consistent with the experimental observations of Funk et al. (1985), who did not observe a sigmoid shape for the release curves obtained with artificial cores made out of any protein shell. Actually, the special conditions imposed by crystallization in the confined inner cavity of ferritin were sufficient to explain these specific shapes.

The sigmoid shape of these curves has most often been attributed to purely biochemical causes. Some authors conjecture, for instance, the presence of two iron types (Jacobs et al., 1989). The first group attached to the interior of the protein, or forming the external layers of the core, would take part in the initial slow step of the reductive release. The second group would then be reduced at a greater rate. The possible influence of phosphate has also been suggested as an explanation for the occurrence of two different mechanisms during iron uptake (Cheng and Chasteen, 1991). Some authors even think that the sigmoid shape may only be due to experimental artifacts (Funk et al., 1985). A physicochemical explanation has been also proposed. The first slow step during iron release could be caused by diffusion of the reducing agent from the exterior toward the interior of the protein, because the latency period is not evidenced for a synthetic core outside of any protein shell (Jones et al., 1978). Nevertheless, a simple calculation shows that the diffusion coefficient should be less than 10^{-16} $m^2 \cdot s^{-1}$ in order to be sensitive to the process (Courteix, 1991). Consequently, this hypothesis cannot be applied to the general case because the diffusive transfer, whether of molecular or Knudsen types, should yield a much higher diffusion coefficient value. In some particular cases, such a hypothesis could therefore be used, recalling that electrostatic interactions could hinder the passage of charged species.

On the contrary, the growth model proposed here explained the occurrence of the sigmoid shape without recourse to any other hypothesis. Nevertheless, even if there is a satisfactory fitting of the whole shape of the experimental curve, it still remains difficult to quantitatively compare the results. The theoretical model has to be improved. For instance, it would be necessary to introduce the variation of the diffusion coefficient with respect to the ferritin content. The molar mass of a ferritin molecule varies by a factor of 2, as n varies from 0 to 4,500, which may result in significant variations of the diffusion coefficient. On the other hand, all the ferritin molecules in a sample do not initially contain strictly the same number of iron atoms. Influence of the initial distribution should also be investigated to improve fitting.

Conclusion

The model fully recovers the experimental variations in uptake and release rates as a function of the number n of iron atoms contained in the molecule. Moreover, it gives a clear explanation of the shape of this curve by correlating its different parts to the successive physicochemical steps that occur throughout crystallization. Unfortunately, it is not possible to firmly identify the shape of the crystal. Nevertheless, it is clear that, if the core is composed of only a small number of different clusters, as suggested by most of the studies, they will have a nearly spherical compact shape.

The sigmoid shape of the iron release curve as a function

of time is also recovered by the model. The constraint imposed by the shell on the crystallization process is sufficient to explain fully the kinetics of iron release by ferritin without recourse to any other hypothesis such as an initiation period induced by some complex physicochemical processes, different iron crystallization types, or an experimental artifact. Also note the gain in computing time achieved by grouping the ferritin population in a small number of large bands. In a general way the model offers an efficient framework for interpreting the crystallization occurring inside a confined space, when the lack of available space significantly affects the behavior of the process and the resulting crystal shape.

Acknowledgments

This research was supported in part by the Société Elf Aquitaine (Groupement de Recherches de Lacq, France). We thank Dr. J.-L. Séris from this company, and Pr. H. Durliat and Pr. M. Comtat from the laboratory for numerous and very helpful discussions.

Notation

C_n = dimensionless concentration of ferritin, $C_n = [\text{Iron}_n]/[\text{FMN}]^0$
C_{Red} = dimensionless concentration of reducing agent (reduced FMN), $C_{\text{Red}} = [\text{Red}]/[\text{FMN}]^0$
D = diffusion coefficient, $m^2 \cdot s^{-1}$
Di = dimensionless diffusivity, $Di = D_{\text{Iron}}/D_{\text{FMN}}$
δ = thin-layer thickness
k_n = rate constant relative to ferritin containing n iron atoms, $m^3 \cdot mol^{-1} \cdot s^{-1}$
K_n = dimensionless rate constant, $K_n = (k_n [\text{FMN}]^0 \delta^2)/D_{\text{FMN}}$
t = time, s
T = dimensionless time, $T = (t D_{\text{FMN}})/\delta^2$
X = dimensionless distance from the electrode, $X = x/\delta$

Literature Cited

Adelmann, T. G., P. Arosio, and J. W. Drysdale, "Multiple Subunits in Human Ferritins: Evidence for Hybrid Molecules," *Biochem. Biophys. Res. Commun.*, **63**, 1056 (1975).

Arasio, P., T. G. Adelmann, and J. W. Drysdale, "On Ferritin Heterogeneity," *J. Biol. Chem.*, **253**, 4451 (1978).

Chasteen, N. D., and E. C. Theil, "Iron Binding by Horse Spleen Apoferritin," *J. Biol. Chem.*, **257**, 7672 (1982).

Cheng, Y. G., and N. D. Chasteen, "Role of Phosphate in Initial Iron Deposition in Apoferritin," *Biochemistry*, **30**, 2947 (1991).

Courteix, A., "Modulation Electrochimique de l'Activité de Proteines à Fer," PhD Thesis, Université Toulouse III, Toulouse, France (1991).

Devaux, R., A. Bergel, and M. Comtat, "Mass Transfer with Chemical Reaction in Thin Layer Electrochemical Reactors," *AIChE J.*, **41**, 1944 (1995).

DiMilla, P. A., J. A. Quinn, S. M. Albelda, and D. A. Lauffenburger, "Measurement of Individual Cell Migration Parameters for Human Tissue Cells," *AIChE J.*, **38**, 1092 (1992).

Durliat, H., and M. Comtat, "Investigation of Electron Transfer between Platinum and Large Biological Molecules by Thin-Layer Spectroelectrochemistry," *Anal. Chem.*, **54**, 856 (1982).

Durliat, H., A. Courteix, A. Bergel, and M. Comtat, "Emploi de la Spectroélectrochimie en Couche Mince pour la Réduction du fer de la Ferritine sur Electrode de Platine," *J. Chim. Phys.*, **90**, 1113 (1993).

Ford, G. C., P. M. Harrison, D. W. Rice, J. M. A. Smith, A. Treffry, J. L. White, and J. Yariv, "Ferritin: Design and Formation of an Iron-Storage Molecule," *Phil. Trans. Roy. Soc. London*, **B304**, 551 (1984).

Funk, F., J. P. Lenders, R. R. Crichton, and W. Schneider, "Reductive Mobilisation of Ferritin Iron," *Eur. J. Biochem.*, **152**, 167 (1985).

Harris, L. R., M. H. Cake, and D. J. Macey, "Iron Release from Ferritin and Its Sensitivity to Superoxide Ions Differs among Vertebrates," *Biochem. J.*, **301**, 385 (1994).

Harrison, P. M., F. A. Fischbach, T. G. Hoy, and G. H. Haggis, "Ferric Oxyhydroxide Core of Ferritin," *Nature*, **216**, 1188 (1967).

Harrison, P. M., T. G. Hoy, I. G. Macara, and R. J. Hoare, "Ferritin Iron Uptake and Release," *Biochem. J.*, **143**, 445 (1974).

Hoffmann, T., and P. M. Harrison, "The Structure of Apoferritin: Degradation into and Molecular Weight of Subunits," *J. Mol. Biol.*, **6**, 256 (1963).

Hoy, G. T., P. M. Harrison, M. Shabbir, and I. G. Macara, "The Release of Iron from Horse Spleen Ferritin to 1, 10 Phenanthroline," *Biochem. J.*, **137**, 67 (1974).

Hubbard, A. T., and F. C. Anson, "Thin Layer Electrochemical Cells," *Electroanalytical Chemistry*, Vol. 4, A. J. Bard, ed., Dekker, New York, p. 129 (1970).

Imai, N., Y. Umezawa, Y. Arata, and S. Fujiwara, "An Electrochemical Study of the Iron Storage Protein, Ferritin," *Biochem. Biophys. Acta*, **626**, 501 (1980).

Jacobs, D. L., G. D. Watt, R. B. Frankel, and G. C. Papaefthymiou, "Redox Reactions Associated with Iron Release from Mammalian Ferritin," *Biochemistry*, **28**, 1650 (1989).

Jones, T., R. Spencer, and C. Walsh, "Mechanism and Kinetics of Iron Release from Ferritin by Dihydroflavins and Dihydroflavin Analogues," *Biochemistry*, **17**, 4011 (1978).

Kadir, F. H. A., F. K. Al-Massad, S. J. A. Fatemi, H. K. Singh, M. T. Wilson, and G. R. Moore, "Electron Transfer between Horse Ferritin and Ferrihaemoproteins," *Biochem. J.*, **278**, 817 (1991).

Kadir, F. H. A., F. K. Al-Massad, and G. R. Moore, "Haem Binding to Horse Spleen Ferritin and its Effects on the Rate of Iron Release," *Biochem. J.*, **282**, 867 (1992).

Kim, K.-J., and E. D. Crandall, "Analysis of Distribution of Water Flow across Alveolar Epithelium," *Biomedical Engineering*, P. Stroeve, R. Jain, and K. Himmelstein, eds., AIChE Symp. Ser., Vol. 227, p. 70 (1983).

Lawson, D. M., A. Treffy, P. J. Artymiuk, P. M. Harrison, S. J. Yewdall, A. Luzzago, G. Cesareni, S. Levi, and P. Arosio, "Identification of the Ferroxidase Centre in Ferritin," *FEBS Lett.*, **254**, 207 (1989).

Lawson, D. M., P. J. Artymiuk, S. J. Yewdall, J. M. A. Smith, J. C. Livingstone, A. Treffy, A. Luzzago, S. Levi, P. Arosio, G. Cesareni, C. D. Thomas, W. V. Shaw, and P. M. Harrison, "Solving the Structure of Human H Ferritin by Genetically Engineering Intermolecular Crystal Contacts," *Nature*, **349**, 541 (1991).

Levi, S., A. Luzzago, G. Cesareni, A. Cozzi, F. Franceschinelli, A. Albertini, and P. Arosio, "Mechanism of Ferritin Iron Uptake: Activity of the H-Chain and Delation Mapping of the Ferro-oxidase Site," *J. Biol. Chem.*, **263**, 18086 (1988).

Lightfood, E. N., *Transport Phenomena and Living Systems*, Wiley, New York (1974).

Macara, I. G., T. G. Hoy, and P. M. Harrison, "The Formation of Ferritin from Apoferritin," *Biochem. J.*, **126**, 151 (1972).

Mann, S., J. V. Bannister, and R. J. P. Williams, "Structure and Composition of Ferritin Cores Isolated from Human Spleen, Limpet (*Patella vulgata*) Hemolymph and Bacterial (*Pseudomonas aeruginosa*) Cells," *J. Mol. Biol.*, **188**, 225 (1986).

Monteiro, H. P., G. F. Vile, and C. C. Winterbourg, *Free Radical Res. Comm.*, **7**, 33 (1989).

Saidel, G. M., and G. M. Burma, "Tracer Species Dynamics for Non-Invasive Evaluation of Pulmonary Blood Flow and Tissue Volume," *Biomedical Engineering*, P. Stroeve, R. Jain, and K. Himmelstein, eds., AIChE Symp. Ser., Vol. 227, p. 43 (1983).

Sirivech, S., E. Frieden, and S. Osaki, "The Release of Iron from Horse Spleen Ferritin by Reduced Flavin," *Biochem. J.*, **143**, 311 (1974).

Steven, M. D., C.-W. Luo, and B. Berner, "Upper and Lower Limits of Human Skin Electrical Resistance in Iontophoresis," *AIChE J.*, **39**, 2011 (1993).

Sun, S., and N. D. Chasteen, "Ferroxidase Kinetics of Horse Spleen Apoferritin," *J. Biol.Chem.*, **267**, 25160 (1992).

Treffry, A., E. R. Bauminger, D. Hechel, N. W. Hodson, I. Nowik, S. J. Yewdall, and P. M. Harrison, "Defining the Role of the Threefold Channels in Iron Uptake, Iron Oxidation and Iron-Core Formation in Ferritin: A Study Aided by Site-Directed Mutagenesis," *Biochem. J.*, **296**, 721 (1993).

Watt, G. D., R. B. Frankel, G. C. Papaefthymiou, K. Spartalian, and E. I. Stiefel, "Redox Properties and Mössbauer Spectroscopy of *Azotobacter vinelandii* Bacterioferritin," *Biochemistry*, **25**, 4330 (1986).

Manuscript received Jan. 12, 1995, and revision received Apr. 26, 1995.